Journal Pre-proof

Effects of particle size and content of RDX on burning stability of RDX-based propellants

Bin-bin Wang, Xin Liao, Luigi T. DeLuca, Wei-dong He

PII: S2214-9147(21)00087-8

DOI: https://doi.org/10.1016/j.dt.2021.05.009

Reference: DT 846

To appear in: *Defence Technology*

Received Date: 27 January 2021

Revised Date: 1 April 2021

Accepted Date: 11 May 2021

Please cite this article as: Wang B-b, Liao X, DeLuca LT, He W-d, Effects of particle size and content of RDX on burning stability of RDX-based propellants, *Defence Technology*, https://doi.org/10.1016/j.dt.2021.05.009.

This is a PDF file of an article that has undergone enhancements after acceptance, such as the addition of a cover page and metadata, and formatting for readability, but it is not yet the definitive version of record. This version will undergo additional copyediting, typesetting and review before it is published in its final form, but we are providing this version to give early visibility of the article. Please note that, during the production process, errors may be discovered which could affect the content, and all legal disclaimers that apply to the journal pertain.

© 2021 China Ordnance Society. Publishing services by Elsevier B.V. on behalf of KeAi Communications Co. Ltd.

Journal Pre-proof

Effects of particle size and content of RDX on burning stability of RDX-based propellants

Bin-bin Wang[a,b]*, Xin Liao[a,b], Luigi T. DeLuca[c], Wei-dong He[a,b]

[a]School of Chemical Engineering, Nanjing University of Science and Technology, Nanjing, 210094, China

[b] Key Laboratory of Special Energy Materials, Ministry of Education, Nanjing, 210094, China

[c] SPLab, Department of Aerospace Engineering, Politecnico di Milano (RET), Milan, I-20156, Italy

* Corresponding author. E-mail: wangbinbin331@163.com

Phone: +86 15195880345, Fax: +86 02584315139

Journal Pre-proof

Journal Pre-proof

Abstract

Particle size and content of RDX are the two main factors that affect the burning stability of RDX-based propellants. However, these effects and the corresponding mechanisms are still controversial. In this work, we investigated the physicochemical processes during burning and the corresponding mechanisms through the technologies of structure compactness analysis on the base of voidage measurement and theoretical interfacial area estimation, apparent burning rate measurement using closed vessel (CV) and extinguished burning surface characterization relying on interrupted closed vessel (ICV) and scanning electron microscope (SEM). The results indicate that the voidage increased with the increase of RDX content and particle size due to the increasing interfacial area and increasing interface gap size, respectively. The apparent burning rate increased with the increase of RDX particle size because of the decreasing RDX specific surface area on the burning surface, which could decrease the heat absorbing rates of the melting and evaporation processes of RDX in the condensed phase. Similarly, the apparent burning rate decreased with the increase of RDX content at pressures lower than around 55 MPa due to the increasing RDX specific surface area. Whereas, an opposite trend could be observed at pressures higher than around 55 MPa, which was attributed to the increasing heat feedback from the gas phase as the result of the increasing propellant energy. For propellants containing very coarse RDX particles, such as 97.8 and 199.4 μm average size, the apparent burning rate increased stably with a flat extinguished surface at pressures lower than around 30 MPa, while increased sharply above around 30 MPa with the extinguished surface becoming more and more rugged as the pressure increased. In addition, the turning degree of *u-p* curve increased with the increase of coarse RDX content and particle size, and could be reduced by improving the structure compactness.

Keywords: RDX particle size and content, structure compactness, apparent burning rate, extinguished surface, burning stability

Journal Pre-proof

Journal Pre-proof

Effects of particle size and content of RDX on burning stability of RDX-based propellants

Abstract

Particle size and content of RDX are the two main factors that affect the burning stability of RDX-based propellants. However, these effects and the corresponding mechanisms are still controversial. In this work, we investigated the physicochemical processes during burning and the corresponding mechanisms through the technologies of structure compactness analysis on the base of voidage measurement and theoretical interfacial area estimation, apparent burning rate measurement using closed vessel (CV) and extinguished burning surface characterization relying on interrupted closed vessel (ICV) and scanning electron microscope (SEM). The results indicate that the voidage increased with the increase of RDX content and particle size due to the increasing interfacial area and increasing interface gap size, respectively. The apparent burning rate increased with the increase of RDX particle size because of the decreasing RDX specific surface area on the burning surface, which could decrease the heat absorbing rates of the melting and evaporation processes of RDX in the condensed phase. Similarly, the apparent burning rate decreased with the increase of RDX content at pressures lower than around 55 MPa due to the increasing RDX specific surface area. Whereas, an opposite trend could be observed at pressures higher than around 55 MPa, which was attributed to the increasing heat feedback from the gas phase as the result of the increasing propellant energy. For propellants containing very coarse RDX particles, such as 97.8 and 199.4 μm average size, the apparent burning rate increased stably with a flat extinguished surface at pressures lower than around 30 MPa, while increased sharply above around 30 MPa with the extinguished surface becoming more and more rugged as the pressure increased. In addition, the turning degree of *u-p* curve increased with the increase of coarse RDX content and particle size, and could be reduced by improving the structure compactness.

Keywords: RDX particle size and content, structure compactness, apparent burning rate, extinguished surface, burning stability

1 Introduction

The nitramines, such as cyclotrimethylene trinitramine (RDX) and cyclotetramethylene tetranitramine (HMX), are widely used in the fields of solid rocket and gun propulsion [1-5]. It is well known that the incorporation of RDX or HMX into propellant formulations could significantly increase the energy level and change the combustion characteristics of the propellants. However, although much work has been devoted to investigating the decomposition and combustion properties of nitramine monopropellants and nitramine propellants [6-11], the knowledge of combustion mechanisms of nitramine propellants, including both physical and chemical processes, is still unsufficient.

In general, for RDX-based propellants, the combustion wave structure can be segmented into three main regions: solid-phase, subsurface liquid-gas phase and gas-phase regimes [11-14]. Many studies have suggested that, during burning, all the RDX in the propellant firstly undergoes a thermodynamic transition to liquid state when the temperature approaches its melting point [15]. Subsequently, rapid decomposition and evaporation of RDX takes place in the subsurface liquid-gas phase [10, 16-18]. Then, the intermediate gasification products of both the RDX and binders continue to oxidize intensely to final gas products in the gas phase, producing enormous energy [6]. In this scenario, the melting, decomposition and evaporation processes of RDX are considered to occur in the condensed phase and the combustion behavior of the RDX-based propellant follows the law of burning in parallel layers. Therefore, the energy to sustain the physiochemical processes of condensed phase mainly includes the heat feedback from the gas phase and heat of

Journal Pre-proof

decomposition, with the effects of heat feedback increasing for increasing combustion pressure [19, 20]. Meanwhile, heat absorption also occurs in the condensed phase due to the endothermic melt and evaporation of RDX. However, in a different scenario it was suggested that, during burning, the coarse RDX particles which were too big to melt, decompose and evaporate in time in the propellant condensed phase would be ejected out to decompose and burn in the gas phase [21, 22]. Consequently, the heat absorption caused by the melting and evaporation processes of RDX would be decreased and the burning surface area would be increased. This conjecture was used to explain why the apparent burning rate increased with the increase of RDX particle size. If the combustion behavior of coarse RDX-based propellant would diverge from the law of burning in parallel layers and the resulting deflagration process would influence the combustion stability. Furthermore, in the apparent burning rate versus pressure curve, there should be a turning point or a sharp increase of apparent burning rate and, intuitively, the corresponding extinguished burning surface should be rugged. However, experimental results are not always in agreement with this conjecture [23-26]. That is, the detailed physiochemical processes during the burning of RDX-based propellants are controversial.

Therefore, this study presents a study on the effects of RDX particle size and content on the burning stability of RDX-based propellants. We focus on the investigations of the physicochemical processes during burning relying on the technologies of structure compactness analysis, apparent burning rate measurement and extinguished burning surface characterization.

2 Materials and Methods

2.1 Materials

Five types of RDX (with mean particle sizes of 3.7, 12.9, 34.3, 97.8 and 199.4 μm, respectively) were obtained from Gansu Yinguang Chemical Industry Group Co., Ltd of China which were produced by synthesis and recrystallization. The particle size distributions and morphologies are shown in Fig. 1 and 2, respectively. Nitrocellulose (NC, 12.6 nitrogen percent), nitroglycerine (NG) and triethyleneglycol dinitrate (TEGDN) were obtained from Luzhou Chemical Industry Group Co., Ltd of China. A series of 15 of NC/NG/TEGDN/RDX propellant formulations based on different particle sizes and contents of RDX were manufactured (Table 1). The basic formulation ZT (6#) selected for this study comprises 59.21% NC, 28.51% NG, 9.67% TEGDN, 2.06% ethyl centralite, 0.55% TiO_2, theoretical force constant (J/g) were calculated using REAL software 3.0. As shown in Table 1, most of the propellants were prepared by conventional solvent method (□) using 25% by mass solutions of acetone and alcohol 50:50, and were made into single-perforated shaped strands with a web size of 1.8 mm using a hydraulic press of 60 tonnes capacity. In order to study the influence of structure compactness on the burning stability, the formulation containing 97.8 μm RDX was also prepared by two special modified methods (□ and □) to increase the structure compactness of the propellant by increasing the extrusion pressure gradually.

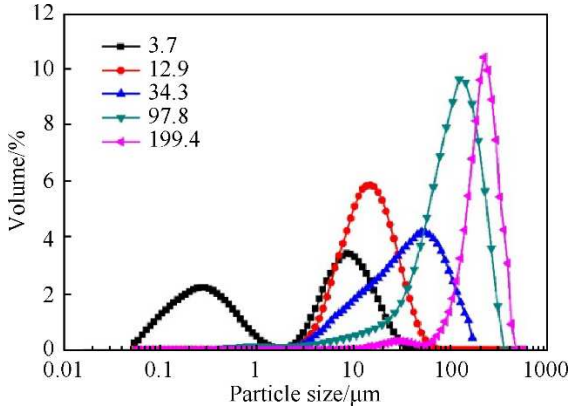

Fig. 1 Particle size distributions of RDX.

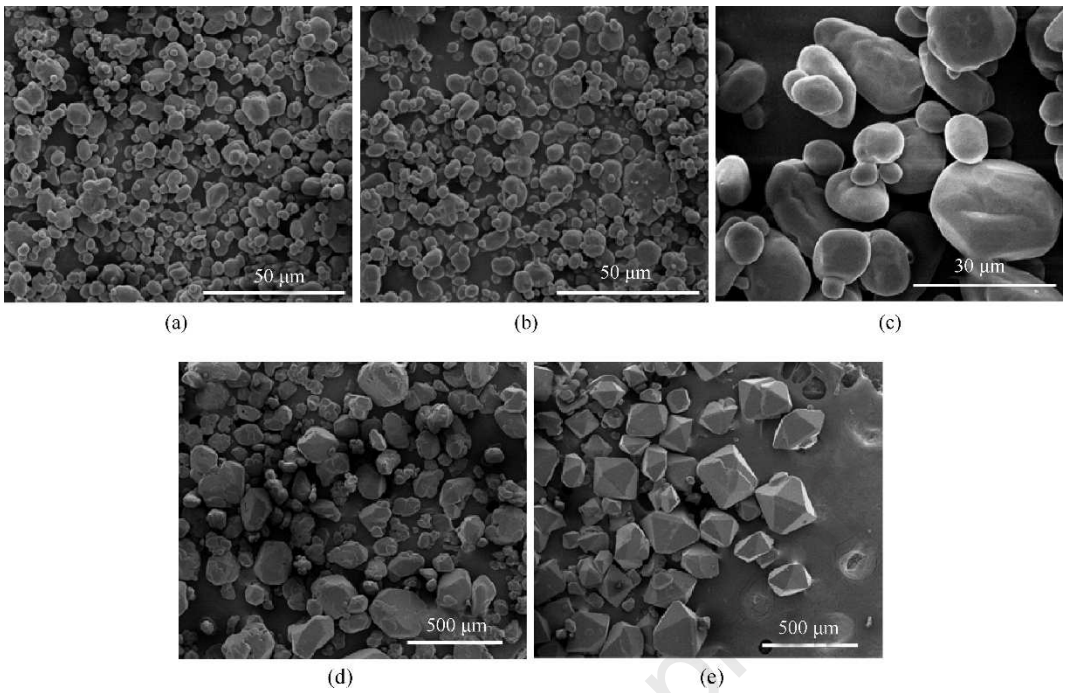

Fig. 2 Morphologies of RDX: (a) 3.7 μm; (b) 12.9 μm; (c) 34.3 μm; (d) 97.8 μm; (e) 199.4μm.

Table 1 Formulations and structure compactness parameters of RDX-based propellants.

No.	Ingredients (mass/%)		Density/(g·cm^{-3})		Voidage	Theoretical	Theoretical	Burning stability
	ZT Binder	RDX /μm	Theoretical	Apparent	(100%)	interfacial area/(cm^2·g^{-1})	force constant/(J·g^{-1})	
1#	70	30 (3.7)	1.675	1.660	0.865	2678.89	1197.63	stable
2#	70	30 (12.9)	1.675	1.659	0.944	1304.20	1197.63	stable
3#	70	30 (34.3)	1.675	1.659	0.958	288.98	1197.63	stable
4#	70	30 (97.8)	1.675	1.624	3.063	97.56	1197.63	unstable
5#	70	30 (199.4)	1.675	1.616	3.494	49.71	1197.63	unstable
6#	100	0	1.613	1.608	0.305	0	1116.34	stable
7#	90	10 (12.9)	1.634	1.628	0.333	434.73	1143.74	stable
8#	80	20 (12.9)	1.654	1.641	0.778	869.46	1170.84	stable
9#	60	40 (12.9)	1.695	1.671	1.448	1738.93	1224.03	stable
10#	90	10 (97.8)	1.634	1.624	0.574	32.52	1116.34	stable
11#	80	20 (97.8)	1.654	1.637	1.053	65.04	1170.84	stable
12#	75	25 (97.8)	1.665	1.643	1.274	81.30	1184.27	poor stable
13#	70	30 (97.8)	1.675	1.649	1.512	97.56	1197.63	poor stable
14#	65	35 (97.8)	1.685	1.648	2.188	113.82	1210.85	unstable
15#	70	30 (97.8)	1.675	1.657	1.038	97.56	1197.63	stable

Note: 1#-9# were prepared by the conventional method □; 10#-14# were prepared by the modified method □; 15# was prepared by the modified method □.

2.2 Methods

The apparent density (ρ_a) measurements of the propellants were carried out using the pycnometer method (MIL-STD-286C, 510.1.1), whereby the densities were determined by comparing the densities of the propellants with the density of water at 15.6 °C. The theoretical density (ρ_t) was estimated based on the following equation:

$$\rho_t = \sum_{i=1}^{n} \omega_i \cdot \rho_i \quad (1)$$

where, ω_i, ρ_i and n are the mass fraction, actual density and total number of the ingredients, respectively.

Then, the voidage (V) was defined by the following expression:

$$V = (1 - \rho_a/\rho_t) \cdot 100\% \quad (2)$$

The theoretical interfacial area (S) per unit mass of the propellant was calculated based on the following formula:

$$S = N \cdot s = [1 \cdot \omega_i/(4 \cdot \pi \cdot R^3 \cdot \rho/3)] \cdot [4 \cdot \pi \cdot R^2] = 3 \cdot \omega_i/(R \cdot \rho) \quad (3$$

where, s, R and ρ are the surface area, radius and density of per RDX particle, respectively. N is the number of RDX particles in per unit mass of the propellant.

The propellant combustion was evaluated in a 100 cm^3 closed vessel (CV) at 20 °C. The test loading density was 0.20 g/cm^3. The ballistic parameters, i.e. apparent burning rate (r), burning rate coefficient (β) and pressure exponent (α), were calculated from the results of CV tests. The propellant apparent burning rate vs. pressure (p) was described in terms of the Vieille' Law:

$$r = \beta \cdot p^{\alpha} \quad (4)$$

The dynamic vivacity (L) was calculated as the following definition (STANAG 4115):

$$L = (\mathrm{d}p/\mathrm{d}t)/(p \cdot p_m)$$

where, t is the burning time, p_m is the maximum combustion pressure.

Rapid extinction of the propellant samples was carried out in an interrupted closed vessel (ICV) (100 cm^3) which could control the extinction pressure by the break-through of a pressureproof copper sheet with different thickness. Consequently, the propellants were suddenly expanded into an evacuated tank which had a thick lining of thermally resistant polyurethane foam on the wall to capture the propellants softly [27]. The thicknesses of the pressureproof copper sheet used in this test were 1.2, 1.5, 1.8, 2.0, 2.5 mm and the corresponding extinction pressures were 26, 48, 75, 100 and 125 MPa, respectively. The morphology of the extinguished propellant surface was characterized by scanning electron microscope (SEM, FEI, Quanta 250 FEG).

3 Results and Discussion

3.1 Structure Compactness Characterizations

The voidage versus RDX content and particle size curves are shown in Fig. 2a and 2b, respectively. The corresponding structure compactness parameters are summarized in Table 1. It can be seen that the RDX content and particle size played a great role on the structure compactness of the RDX-based propellant. From Table 1 and Fig. 2a, one can find that the density of the RDX-based propellant increased with the increase of RDX content. Unexpectedly, the corresponding voidage of the propellant increased at the same time because of the increasing number of the interface between ZT binder and RDX particle (Table 1). On the other hand, from Table 1 and Fig. 2b, one can see that the density of the RDX-based propellant decreased with the increasing of RDX particle size and, especially, when the particle size is larger than 34.3 μm, the voidage increased sharply. This is mainly due to the fact that, although the theoretical interfacial area decreased with the increase of RDX particle size, the adhesive force of ZT binder to RDX particle was decreased because of the RDX particle size larger than the NC fiber diameter [28]. As a result, the gap size of the interface was increased. That is, the structure compactness of the propellant prepared by conventional method decreased with the increasing of the RDX content and particle size. Interestingly, when the extrusion pressure was increased gradually, the density of the propellant containing 97.8 μm RDX particles was increased and the voidage was decreased effectively.

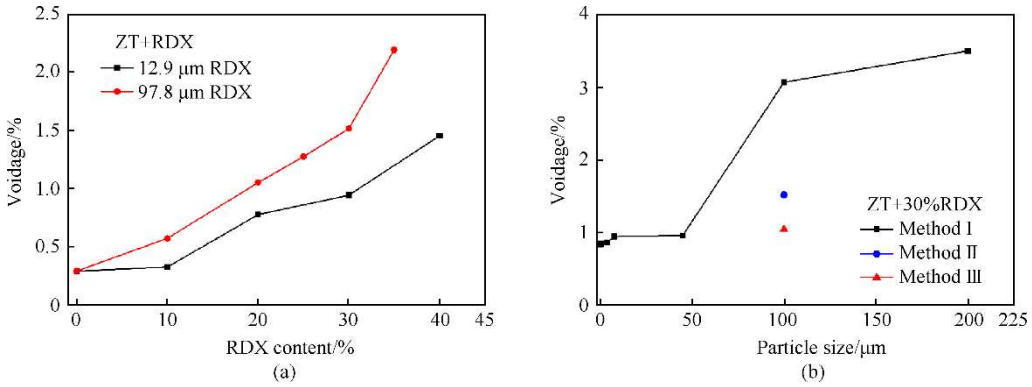

Fig. 3 The voidage versus RDX content and particle size curves of RDX-based propellants.

3.2 Burning Properties

Fig. 4a and 4b show the *u*-*p* curves and *L*-*p*/p_m curves of the RDX-based propellants containing different particle sizes of RDX (30% by mass), respectively. From Fig. 4a, one can see that the apparent apparent burning rate increased with the increase of RDX particle size. This can be attributed to the expection that, for RDX-based propellant of which the melt, decomposition and evaporation processes of RDX were considered to occur in condensed phase, when the RDX particle size was increased, the RDX specific suface on the burning surface was decreased, resulting in the decrease of the heat absorbing rates of the RDX melt and evaporation processes in condensed phase. Therefore, the heat to sustain the degradation of RDX and binder was increased and the apparent burning rate was increased. On the other hand, the apparent burning rates of the propellants containing 3.7, 12.9, 34.3 μm RDX particles increased stably with the increase of pressure, while the apparent burning rates of the propellants containing 97.8 and 199.4 μm RDX particles increased sharply above around 30 MPa. From Fig. 4b, for the propellants containing 97.8 and 199.4 μm RDX particles, an abrupt increase of the *L*-*p*/p_m curve is also observed after p/p_m = 0.15 approximately, which is not in agreement with the neutral burning behavior of propellant with single-perforation structure, like those of the propellants containing 3.7, 12.9, 34.3 μm RDX particles. This is dangerous for high-pressure weapons or rockets because, if the initial chamber pressure is too high or increases too fast, it can result in bore premature or even worse accident. A probable reason for this deflagration phenomenon is that the structures of the 97.8 and 199.4 μm RDX-based propellants were very loose, according to the voidage results as described above, and the erosion from the gas phase to the interface gap between RDX and binder on the burning surface was intensified with the increase of pressure [22]. Thus, the 97.8 and 199.4 μm RDX particles could be ejected out from the condensed phase of the propellants to decompose and burn in the gas phase above around 30 MPa.

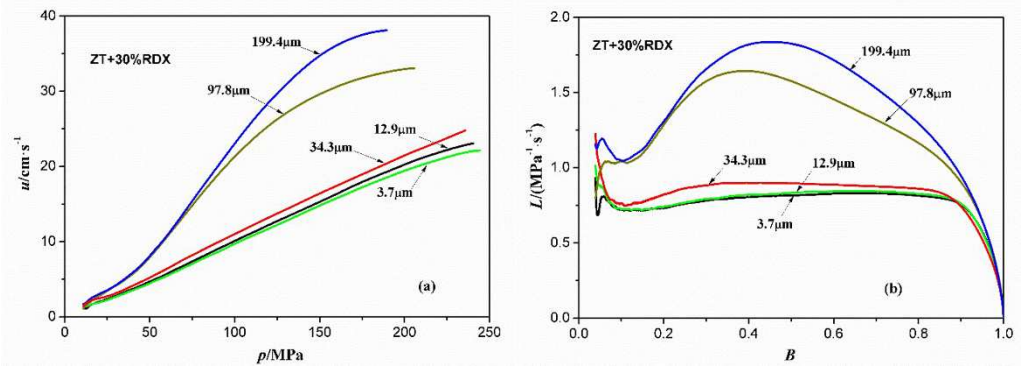

Fig. 4 *u*-*p* curves and *L*-*p*/p_m curves of 30% RDX-based propellants containing different particle sizes of RDX.

Fig. 5 presents the *u*-*p* curves of the RDX-based propellant containing different contents of 12.9 μm RDX particles. It can be seen that the apparent burning rates of the propellants containing 0%, 10%, 20%, 30% and 40% 12.9 μm RDX particles increased stably with the increase of pressure, implying that the 12.9 μm RDX particles melts, decomposes and evaporates in the condensed phase of the propellant. In addition, the apparent burning rate decreased with the increase of

RDX content at pressures lower than around 55 MPa, while there was an opposite trend when the pressure was higher than 55 MPa approximately. Surprisingly, the apparent burning rate of the propellant containing 10% RDX was alway lower than that of the ZT propellant. The influence of RDX content on the apparent burning rate is mainly due to the fact that when the RDX content was increased, the RDX heat absorption in the condensed phase was increased, resulting in the decrease of the apparent burning rate at low pressures. On the other hand, the heat feedback from the gas phase increased with the increase of RDX content because of the increasing energy of the propellant (as shown in Table 1) at the same time, especially at high pressures. Therefore, the apparent burning rate was increased at high pressures. This further reveals the importance of the endothermic melting and evaporation process of RDX in the condensed phase on the combustion properties of RDX-based propellants.

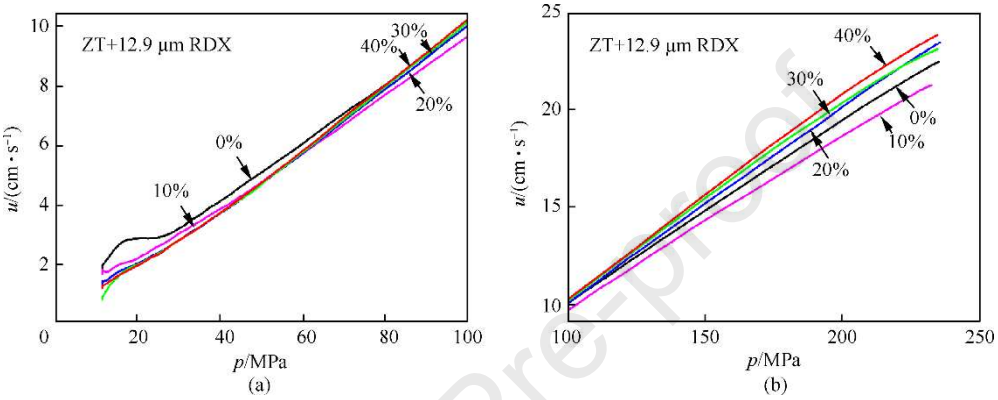

Fig. 5 *u-p* curves of the 12.9 μm RDX-based propellant containing different mass fractions of RDX.

Fig. 6a and 6b show the *u-p* curves and L-p/p_m curves of the RDX-based propellants containing different contents of 97.8 μm RDX particles, respectively. From Fig. 6a, one can see that, for 97.8 μm RDX-based propellants, the turning degree of *u-p* curve around 30 MPa increased with the increase of RDX content. This can be attributed to the fact that the compactness of the 97.8 μm RDX-based propellant became looser when the RDX content was increased and herein, the percent of coarse RDX which could be ejected out from the condensed phase to decompose and burn in the gas phase above around 30 MPa was increased. From Fig. 6b, one can find that, when the RDX content was increased, the L-p/p_m curve gradully diverged from the neutral burning law of propellant with single-perforation structure like that of the ZT propellant, which indicates a burning instability of 97.8 μm RDX-based propellant.

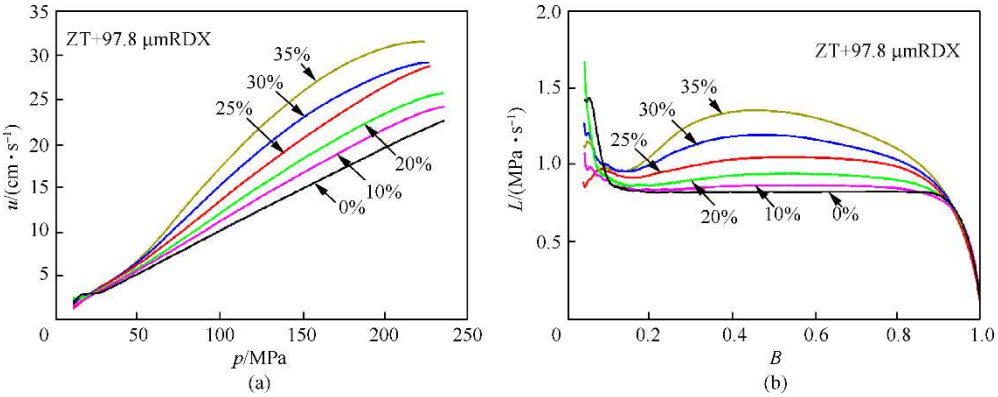

Fig. 6 *u-p* curves and L-p/p_m curves of 97.8 μm RDX-based propellant containing different mass fractions of RDX.

To further testify the influence of the structure compactness on the burning stability, the *u-p* curves and L-p/p_m curves of three RDX-based (97.8 μm RDX, 30% by mass) propellants with different voidages are displayed in Fig. 7. From Fig. 7a one can see that, when the pressure was lower than 30 MPa approximately, the apparent burning rates of the three propellants were similar and increased stably with the increase of pressure, while, above 30 MPa, the curve turning

degree of the *u-p* curve increased with the increase of propellant voidage. Interestingly, when the the structure compactness was high enough, the *u-p* curve of the 97.8 μm RDX-based propellant with the voidage of 1.038% could increase stably without turning point, like those of the propellants containing 3.7, 12.9, 34.3 μm RDX. In this case, the 97.8 μm RDX particles are believed to melt, decompose and evaporate in the condensed phase of the propellant with the voidage of 1.038%. This can be further confirmed by the L-p/p_m curves (Fig. 7b). One can see that, when the propellant voidage was increased, the extent of the abrupt increase of L-p/p_m curve at the early process became more serious whereas the L-p/p_m curve of the propellant with the voidage of 1.038% is observed in great agreement with the neutral burning law of propellant with single-perforation structure.

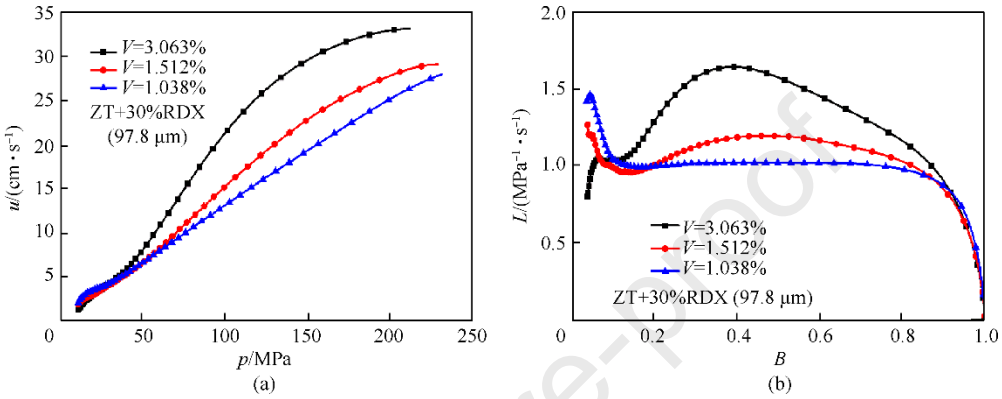

Fig. 7 *u-p* curves and L-p/p_m curves of 30% 97.8 μm RDX-based propellant with different voidages.

3.3 Extinguished Burning Surface Characterizations

To further validate the physiochemical processes during burning of the examined RDX-based propellants, samples of these propellants were subjected to the rapid extinction analyses. Fig. 8 ~ Fig. 11 illustrate the SEM images of the raw surfaces and extinguished surfaces subjected to extinction pressure (125 MPa) of the 3.7, 12.9, 34.3, 199.4 μm RDX-based propellants, respectively. From Fig. 8 ~ Fig. 10, one can see that there were many irregularly RDX recrystallization particles on the extinguished surfaces of the 3.7, 12.9, 34.3 μm RDX-based propellants which were melting before rapid extinction and different from the RDX morphologies on the raw surfaces. Nevertheless, from Figure 10, one can see that there were many big holes on the extinguished surfaces of the 199.4 μm RDX-based propellant and these holes were slightly bigger than the original RDX on the raw surfaces. These phenomena were in great agreement with the burning rate results and confirmed the corresponding conjecture above.

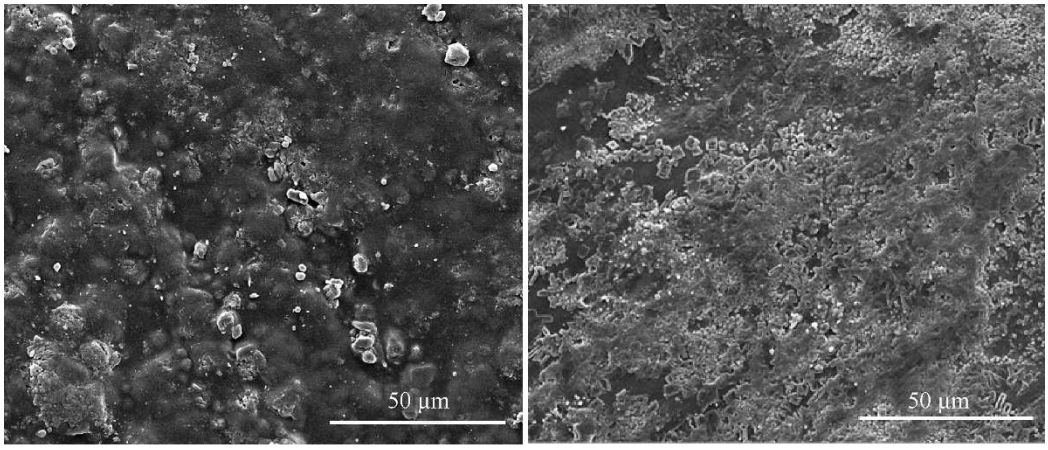

Fig. 8 SEM images of the 3.7 μm RDX-based propellant: (a) raw surface; (b) extinguished surface (125 MPa).

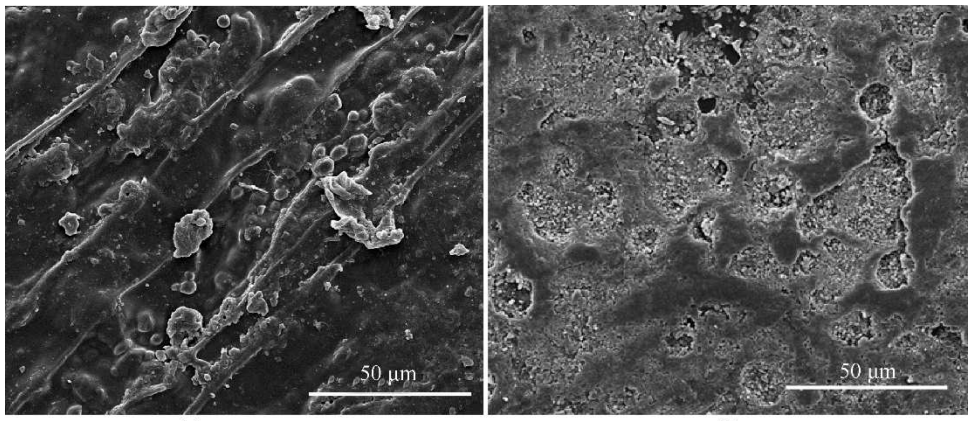

Fig. 9 SEM images of the 12.9 μm RDX-based propellant: (a) raw surface; (b) extinguished surface (125 MPa).

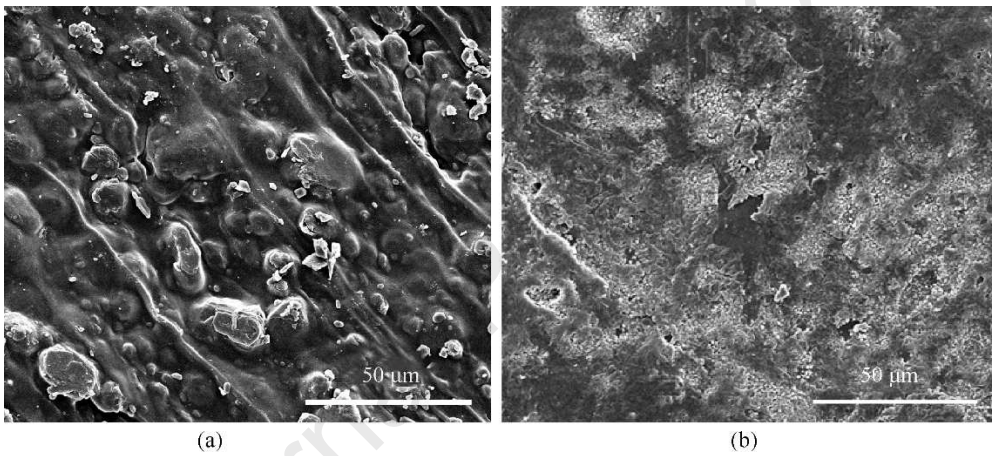

Fig. 10 SEM images of the 34.3 μm RDX-based propellant: (a) raw surface; (b) extinguished surface (125 MPa).

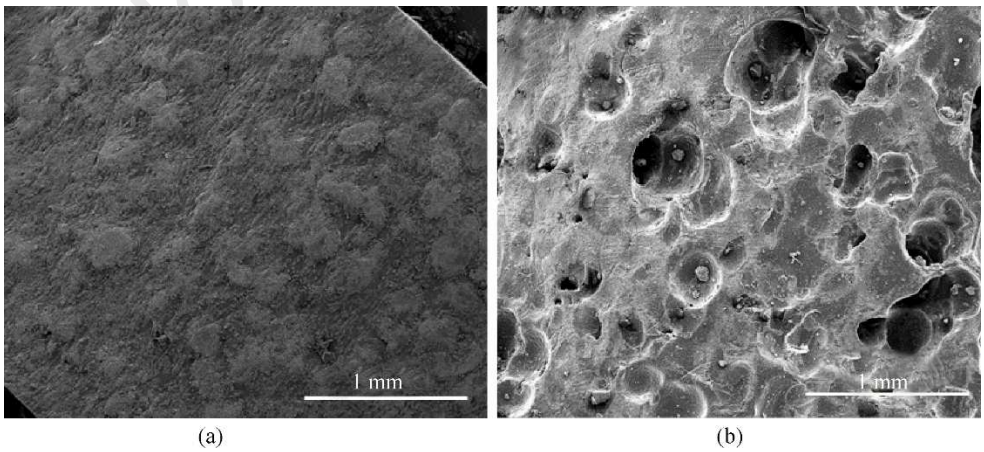

Fig. 11 SEM images of the 199.4 μm RDX-based propellant: (a) raw surface; (b) extinguished surface (125 MPa).

Fig. 12 illustrates the SEM images of the extinguished surfaces of the 97.8 μm RDX-based propellants with the voidage of 3.063%, which were subjected to different extinction pressures (26, 48, 75, 100 and 125 MPa). It can be seen that the extinguished propellant surface extinguished under 26 MPa was relatively flat with only some small holes which were much smaller than 97.8 μm. However, when the extinction pressure was increased, the extinguished surface became more and more rugged, and some big holes larger than 97.8 μm appeared on the surface. Noticeably, the size and number

of these holes increased with the increase of the extinction pressure. These phenomena are in great agreement with the ballistic results as described above.

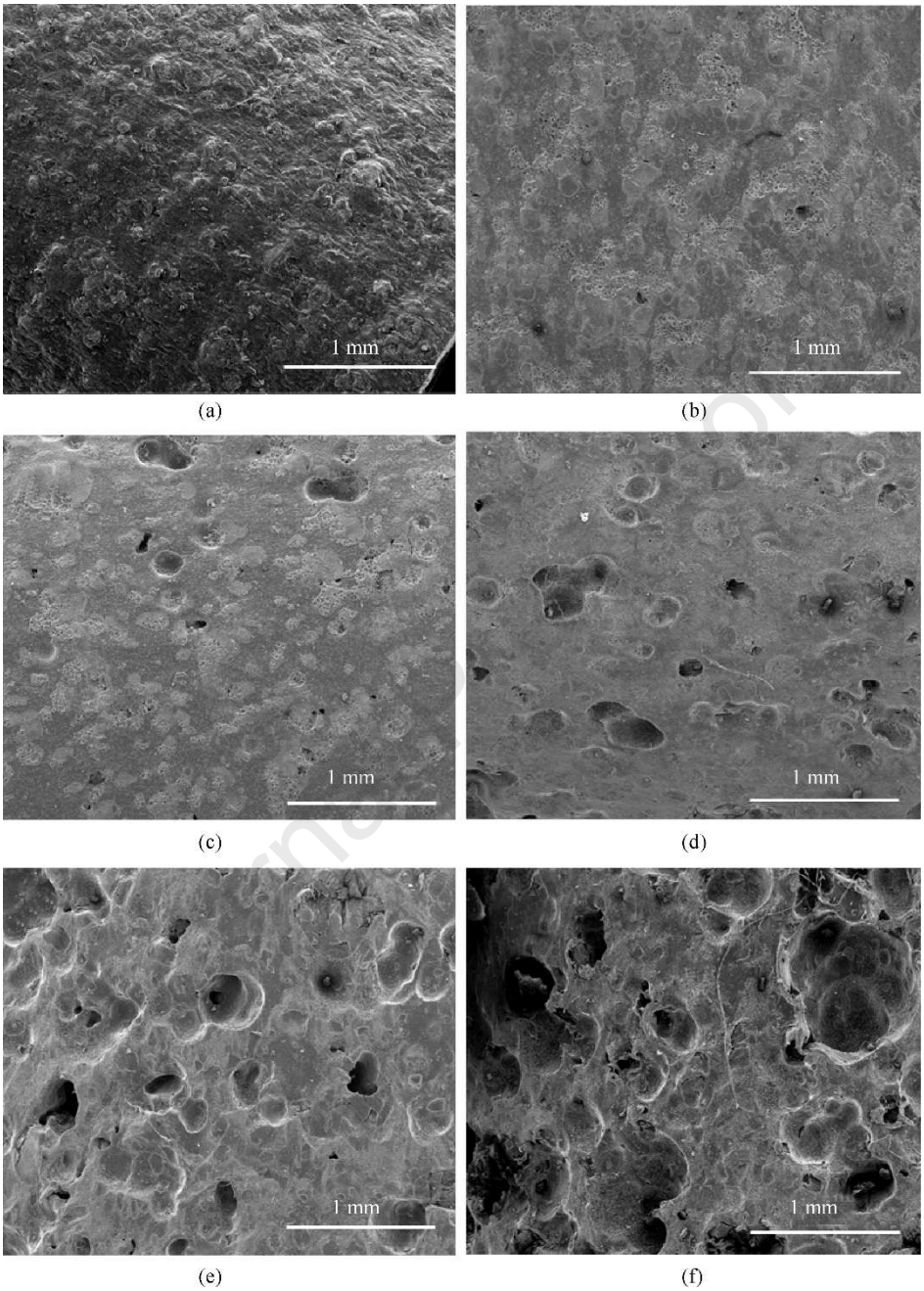

Fig. 12 SEM images of the extinguished surfaces of the 97.8 μm RDX-based propellant with the voidage of 3.063%: (a) raw, (b) 26 MPa, (c) 48 MPa, (d) 75 MPa, (e) 100 MPa, (f) 125 MPa.

Additionally, the SEM images of the extinguished surfaces of the 97.8 μm RDX-based propellant with the voidages of 1.512% and 1.038%, which were subjected to the extinction pressure of 125 MPa are presented in Fig. 13. From Fig. 12f and Fig. 13, one can see that the extinguished surface became more and more flat when the compactness of the 97.8 μm RDX-based propellant was increased. Interestingly, the extinguished surface of the 97.8 μm RDX-based propellant with the voidages of 1.038% was flat and there were no large holes on the surface, even when it was extinguished at 125 MPa. This further confirms that the RDX content and particle size, together with the compactness of the propellant, are all important factors that influence the burning stability of the RDX-based propellant.

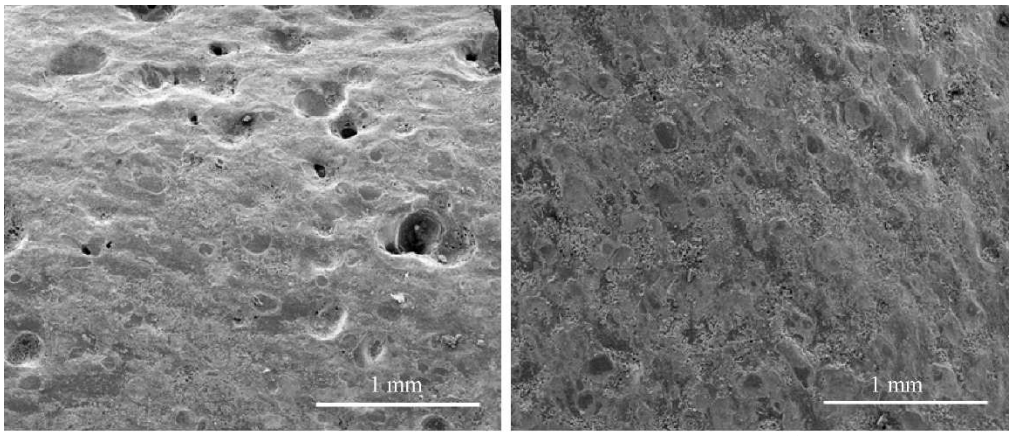

(a) (b)

Fig. 13 SEM images of the extinguished surfaces (125 MPa) of the 97.8 μm RDX-based propellant with different voidages: (a) 1.512%, (b) 1.038%.

4 Conclusions

In this paper, the effects of RDX particle size and content on the burning stability of RDX-based propellants and the corresponding physicochemical processes during burning were investigated. The following conclusions can be made:

(1) The structure compactness of the propellant prepared by conventional methods decreased with the increasing of the RDX content due to the increasing number of the interface between ZT binder and RDX particle. On the other hand, although the theoretical interfacial area was decreased with the increase of RDX particle size, the adhesive force of ZT binder to RDX particle was decreased because of the RDX particle size larger than the NC fiber diameter. As a result, the gap size of the interface was increased and the corresponding structure compactness of the propellant prepared by conventional method was decreased.

(2) The apparent burning rate increased with the increase of RDX particle size. This is because when the particle size of RDX was increased, the RDX specific surface area on the burning surface was decreased, resulting in the decrease of the heat absorbing rates of the melting and evaporation processes of RDX in the condensed phase. Therefore, the heat to sustain the degradation of RDX and binder was increased and the apparent burning rate was increased.

(3) The apparent burning rate decreased with the increase of RDX content at pressures lower than around 55 MPa, while there was an opposite trend at pressures higher than 55 MPa approximately. This is due to the fact that when the RDX content was increased, the RDX heat absorption in the condensed phase was increased, resulting in a decrease of the apparent burning rate at low pressures. On the other hand, the heat feedback from the gas phase increased with the increase of RDX content because of the increasing propellant energy, especially at high pressures, resulting in an increase of the apparent burning rate at high pressures.

(4) For propellants containing very coarse RDX particles, such as 97.8 and 199.4 μm RDX average size, the apparent burning rates increased stably at pressures lower than around 30 MPa, while increased sharply above around 30 MPa, and the turning degree of *u*-*p* curve increased with the increase of RDX content and particle size. On the contrary, the apparent burning rates of the propellants containing fine RDX particles, such as 3.7, 12.9, 34.3 μm RDX average size, increased stably with the increase of pressure in the whole pressure interval. This can be attributed to the fact that the compactness of the coarse RDX-based propellant became looser when the RDX content and particle size were increased, and the erosion from the gas phase to the interface gap between RDX and binder on the burning surface was intensified with the pressure increase. Herein, coarse RDX could be ejected out from the condensed phase to decompose and burn in the gas phase above around 30 MPa.

(5) The extinguished propellant surface of the 97.8 μm RDX-based propellant was flat when the extinction pressure

was lower than around 30 MPa, while it became more and more rugged (with some big holes larger than 97.8 μm on the surface) when the extinction pressures were higher than around 30 MPa. Interestingly, the extinguished surface became more and more flat when the compactness of the 97.8 μm RDX-based propellant was improved by increasing the extrusion pressure gradually. That is, the burning stability of RDX-based propellant could be improved by increasing the structure compactness. This is in great agreement with the combustion phenomena as discussed in this paper.

Acknowledgements

The authors would like to acknowledge the support of Key Laboratory of Special Energy Materials, Ministry of Education, Nanjing, 210094, China.

References

[1] Damse R, Singh H. Nitramine-based high energy propellant compositions for tank guns. Defence Science Journal 2000; 50(1): 75-81.

[2] Sanghavi RR, Kamale PJ, Shaikh MA, et al. HMX based enhanced energy LOVA gun propellant. J Hazard Mater 2007; 143(1-2): 532-534.

[3] Pillai A, Dayanandan C, Gandhe B, et al. Studies on some nitramine based low vulnerability ammunition propellants with cellulose acetate as a binder . Defence Science Journal 1996; 46(2): 77.

[4] Chakraborthy TK, Raha KC, Omprakash B, et al. A study on gun propellants based on Butyl-NENA. Journal of Energetic Materials 2004; 22(1): 41-53.

[5] Xiao LQ, Fan XZ, Li JZ, et al. Effect of Al content and particle size on the combustion of HMX-CMDB propellant. Combustion and Flame 2020; 214:80-89.

[6] Yetter RA, Dryer FL, Allen MT, et al. Development of gas-phase reaction-mechanisms for nitramine combustion. Journal of Propulsion and Power 1995; 11(4): 683-697.

[7] Oxley J, Kooh A, Szekeres R, et al. Mechanisms of nitramine thermolysis. The Journal of Physical Chemistry 1994; 98(28): 7004-7008.

[8] Kim E, Yang V, Liau YC. Modeling of HMX/GAP pseudo-propellant combustion. Combustion and Flame 2002; 131(3): 227-245.

[9] Davidson JE, Beckstead MW. Improvements to steady-state combustion modeling of cyclotrimethylenetrinitramine. Journal of Propulsion and Power 1997; 13(3): 375-383.

[10] Palopoli SF, Brill TB. Thermal-decomposition of energetic materials .52. on the foam zone and surface-chemistry of rapidly decomposing HMX. Combustion and Flame 1991; 87(1): 45-60.

[11] Alexander MH, Dagdigian PJ, Jacox ME, et al. Nitramine propellant ignition and combustion research. Progress in Energy and Combustion Science 1991; 17(4): 263-296.

[12] Schroeder M, Fifer R, Miller M, et al. Condensed-phase processes during combustion of solid gun propellants. I. nitrate ester propellants. Combustion and Flame 2001; 126(1): 1569-1576.

[13] Beckstead M, Yang V, Puduppakkam KV. Modeling and simulation of combustion of solid propellant ingredients using detailed chemical kinetics. 40th AIAA/ASME/SAE/ASEE Joint Propulsion Conference Proceedings 2004;1-19;

[14] Yoon JK, Thakre P, Yang V. Modeling of RDX/GAP/BTTN pseudo-propellant combustion. Combustion and Flame 2006; 145(1-2): 300-315.

[15] Naya T, Kohga M. Influences of particle size and content of RDX on burning characteristics of RDX-based propellant. Aerospace Science and Technology 2014; 32(1): 26-34.

Journal Pre-proof

[16] Schroeder M, Fifer R, Miller M, et al. Condensed-phase processes during combustion of solid gun propellants. II. nitramine composite propellants. Combustion and Flame 2001; 126(1): 1577-1598.

[17] Zenin A. HMX and RDX - Combustion mechanism and influence on modern double-base propellant combustion. Journal of Propulsion and Power 1995; 11(4): 752-758.

[18] Tsang W, Herron JT. Chemical kinetic data base for propellant combustion I. Reactions involving NO, NO2, HNO, HNO2, HCN and N2O. Journal of Physical and Chemical Reference Data 1991; 20(4): 609-663.

[19] Miller MS, Anderson WR. Burning-rate predictor for multi-Ingredient propellants: nitrate-ester propellants. Journal of Propulsion and Power 2004; 20(3): 440-454.

[20] Kubota N. Combustion mechanisms of nitramine composite propellants. Symposium (International) on Combustion Proceedings 1981; 18(1): 187-194.

[21] Galler RZ. Correlations between deflagration characteristics and surface properties of nitramine-based propellants. AIAA Journal 1968; 6(11): 2107-2110.

[22] Cohen NS, Price CF. Combustion of nitramine propellants. Journal of Spacecraft and Rockets 1975; 12(10): 608-612.

[23] Pillai A, Sanghavi R, Dayanandan C, et al. Studies on RDX particle size in LOVA gun propellant formulations. Propellants, Explosives, Pyrotechnics 2001; 26(5): 226-228.

[24] Joshi M, Dayanandan C, Pillai A, et al. Role of bimodal RDX in LOVA gun propellant combustion. Defence Science Journal 1998; 48(3): 317.

[25] Cohen NE. Combustion characteristics of advanced nitramine-based propellants. Symposium (International) on Combustion Proceedings 1981; 18(1): 195-206.

[26] Pillai A, Dayanandan C, Joshi M, et al. Studies on the effects of RDX particle size on the burning rate of gun propellants. Defence Science Journal 1996; 46(2): 83-86.

[27] Birk A, Guercio MD, Kinkennon A, et al. Interrupted-burning tests of plasma‐Ignited JA2 and M30 grains in a closed chamber. Propellants, Explosives, Pyrotechnics 2000; 25(3): 133-142.

[28] Wang B, Liao X, Wang Z, et al. Preparation and Properties of a nRDX-based Propellant. Propellants Explosives Pyrotechnics 2017; 42(6): 649-658.

Journal Pre-proof

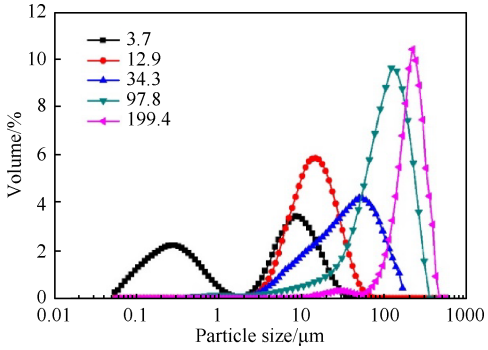

Journal Pre-proof

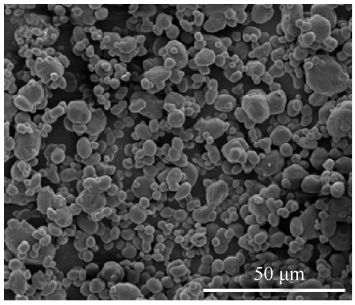

(a)

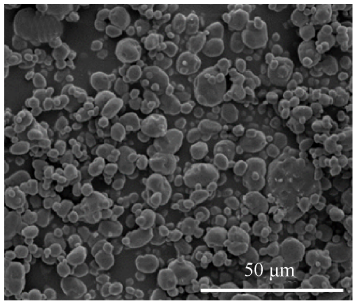

(b)

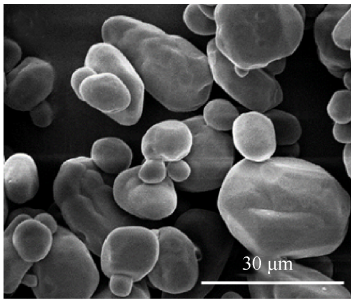

(c)

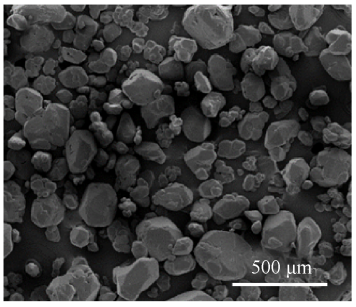

(d)

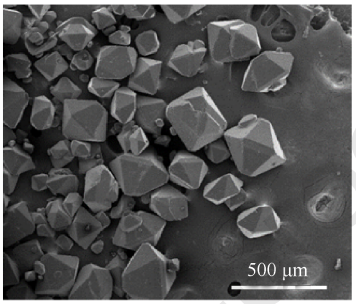

(e)

Journal Pre-proof

Journal Pre-proof

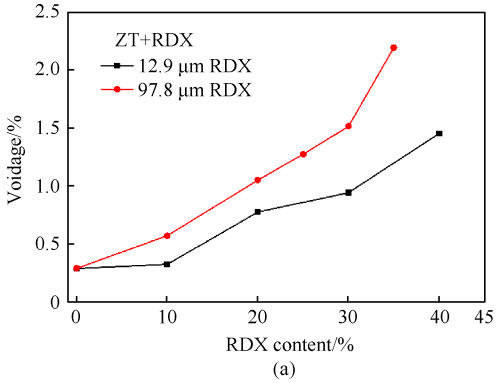

(a)

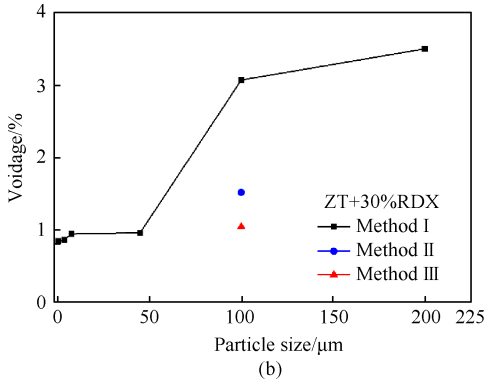

(b)

Journal Pre-proof

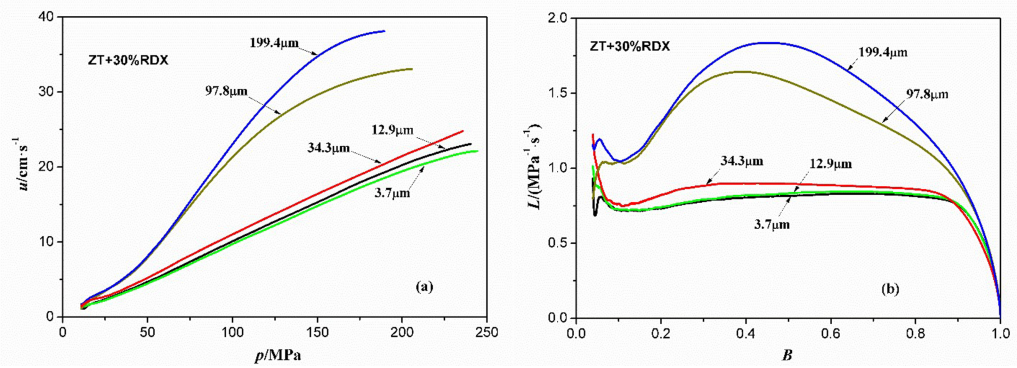

Journal Pre-proof

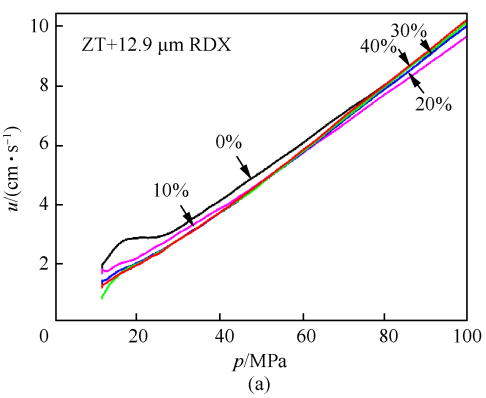

(a)

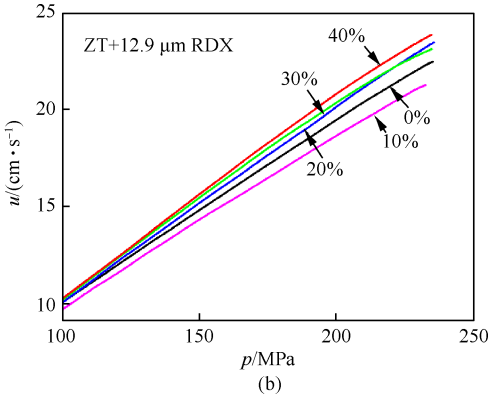

(b)

Journal Pre-proof

Journal Pre-proof

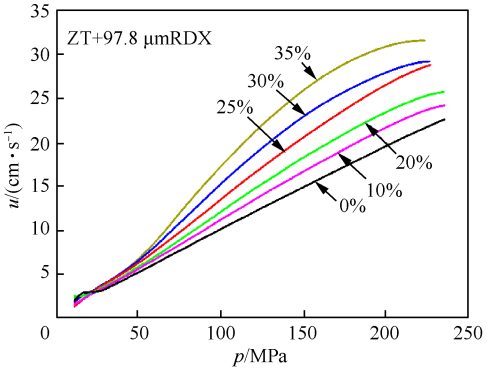

(a)

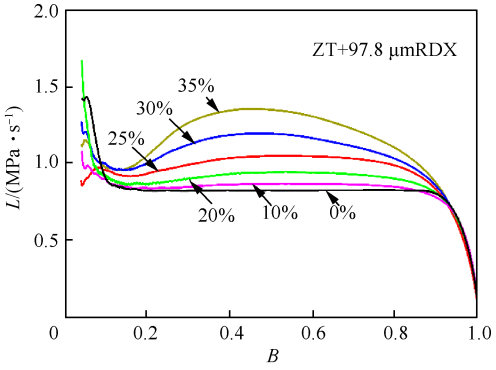

(b)

Journal Pre-proof

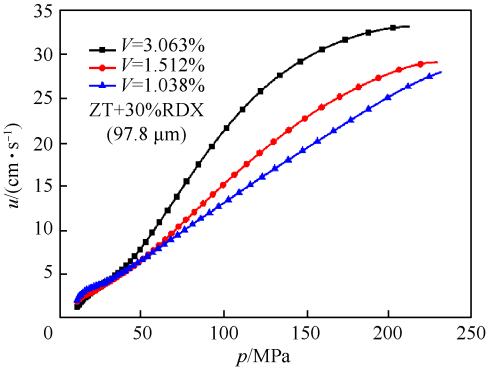

(a)

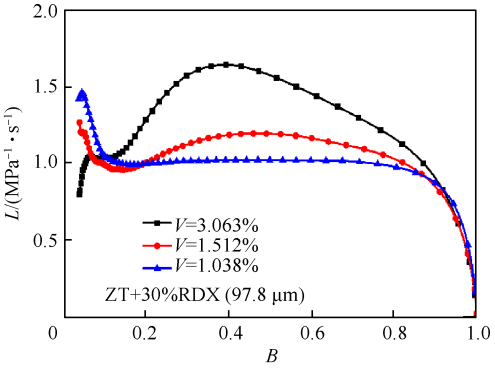

(b)

Journal Pre-proof

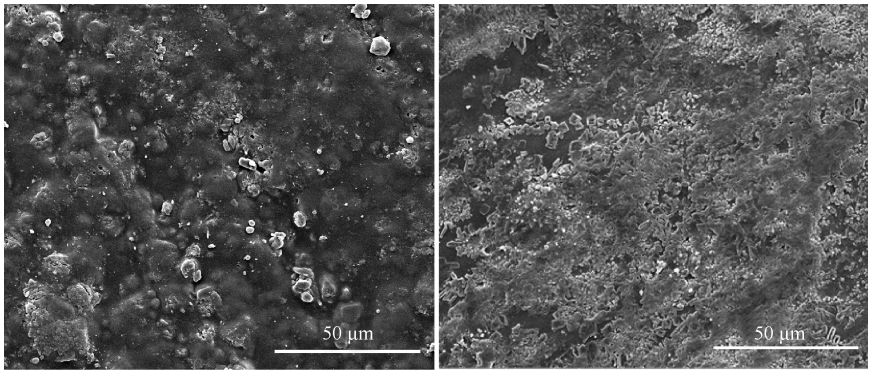

(a) (b)

Journal Pre-proof

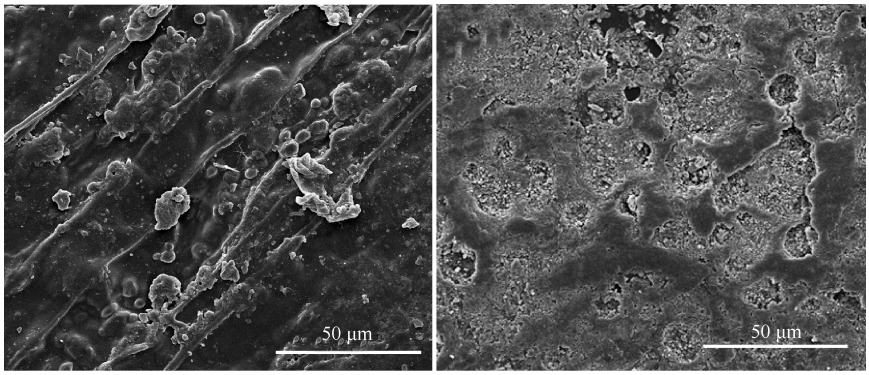

(a) (b)

Journal Pre-proof

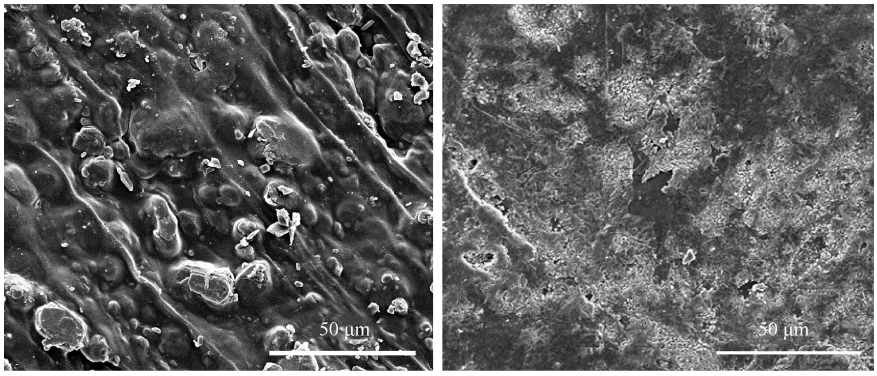

(a) (b)

Journal Pre-proof

Journal Pre-proof

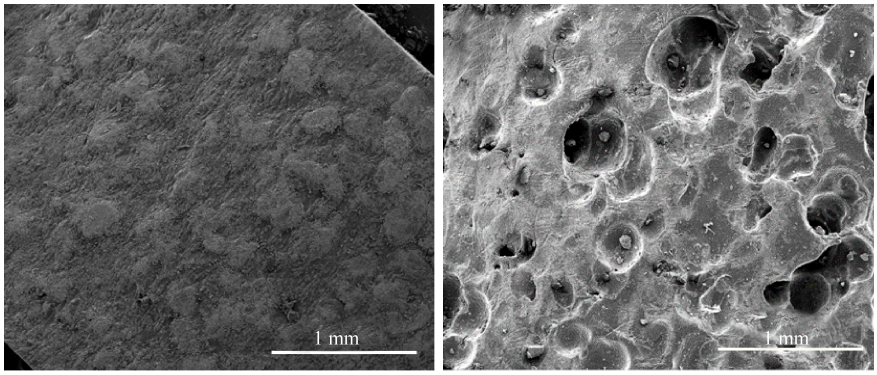

(a) (b)

Journal Pre-proof

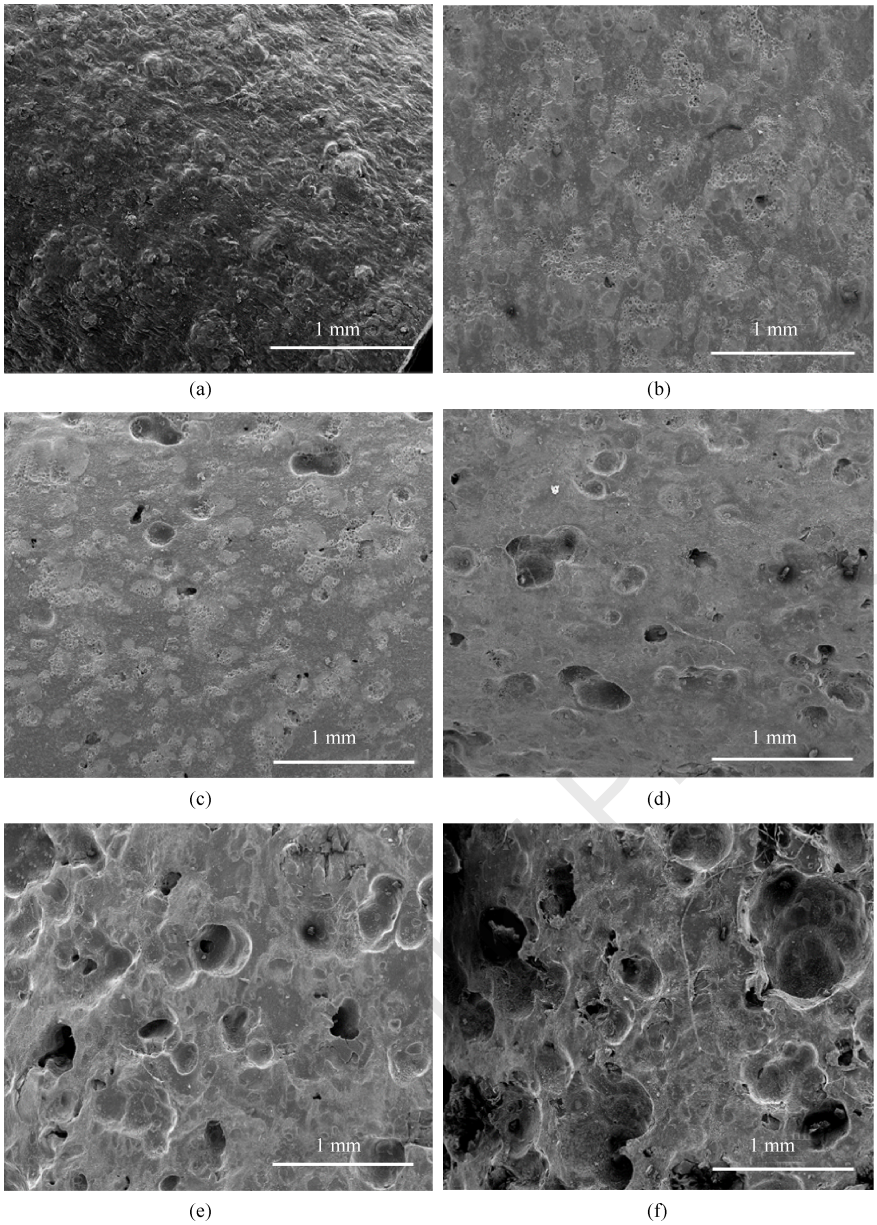

(a) (b)

(c) (d)

(e) (f)

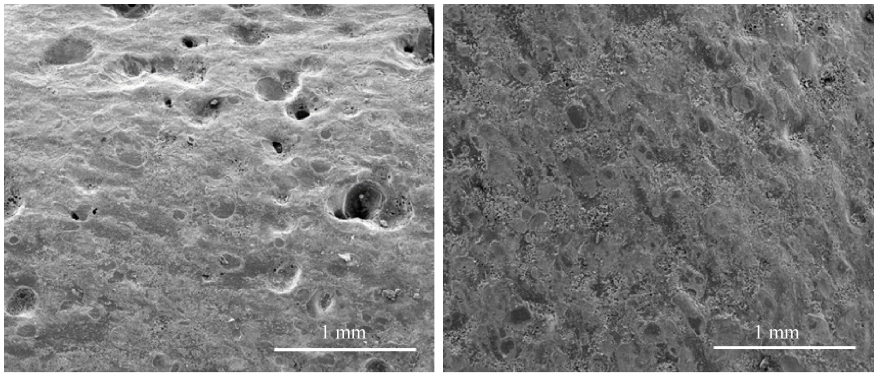

(a) (b)

Journal Pre-proof